Supplementary Information for

Unveiling the relationship between the multilayer structure of metallic MoS_2 and the cycling performance for lithium ion batteries

Zhipeng Liu, Kaiwen Wang, Guoqing Huang, Shuyi Yu, Xiaotian Li, Nan Li, Kaifeng Yu**

Key Laboratory of Automobile Materials (Ministry of Education), School of Materials Science and Engineering, Jilin University, 2699 Qianjin Street, Changchun, 130012, P. R. China

Experimental section

1. Synthesis of samples

For the preparation of the 1T-MoS_2/Ti electrode, 12 mg of molybdenum trioxide (MoO_3) and 50 mg of sodium sulfide ($NaS_2 \cdot 9H_2O$) were dissolved in 24 mL of deionized water and stirred for 10 min to get a homogeneous solution. Afterwards, 30 mg of thioacetamide (CH_3CSNH_2) and 120 mg of urea ($CO(NH_2)_2$) were added to the solution. Then, the solution was transferred into a 50-mL Teflon-lined stainless autoclave. A piece of Ti foil (2 cm × 3cm), which was previously rinsed successively with 3 M HCl, deionized water, and ethanol, was immersed in the solution. The autoclave was sealed and heated in an oven at 200 °C for 12 h. After cooling to room temperature, the Ti foil was rinsed thoroughly with deionized water, ethanol, and carbon disulfide (CS_2) several times and dried in a vacuum at 60 °C. For comparison, a 2H-MoS_2/Ti electrode was prepared by annealing the as-obtained 1T-MoS_2/Ti in Ar flow at 350 °C for 2h.

2. Characterization

Raman spectra were collected on a micro-Raman spectrometer (Renishaw) with a laser of 532 nm wavelength at 0.2 mW. X-ray photoelectron spectroscopy (XPS) analyses were conducted on an ESCALAB 250 electron spectrometer with an Al Kα radiation source (hν = 1486.6 eV). The microstructure and morphology of samples were observed through scanning electron microscopy (SEM, JEOL JSM-6700F), transmission electron microscopy (TEM, JEOL JEM-2100F), and high-angle annular dark-field scanning transmission electron microscopy (HAADF-STEM, JEOL JEM-

ARM300F GRAND ARM with aberration correctors). TEM samples were prepared by desquamating MoS_2 nanosheets from Ti foils through ultrasonic treatment.

3. Electrochemical Testing

The 2025-type coin cells were assembled in an argon-filled glove box. The as-synthesized 1T-MoS_2 electrode (diameter of 12 mm) was directly served as the working electrode and a pure lithium foil as the counter electrode. A solution of 1M $LiPF_6$ dissolved in ethylene carbonate (EC)/dimethyl carbonate (DMC) (1:1 by volume) was utilized as the electrolyte, and a Celgard 2500 membrane was chosen as the separator. The cycling test of cells was performed on a CT2001A LAND multi-channel battery tester by sweeping between 3 and 0.01vs Li^+/Li. Cyclic voltammetry curves were obtained on a PARSTAT 3000A-DX electrochemical working station with a scan rate of 0.2 $mV \cdot s^{-1}$ at a voltage range of 0.01 to 3 V vs Li^+/Li.

4. Computational details

All calculations were performed based on density function theory (DFT) by using the Cambridge Sequential Total Energy Package (CASTEP). The electronic exchange-correlation energy was treated by the spin-polarized, generalized-gradient approximation of Perdew–Burke–Ernzerhof (PBE). The models of lithiated MoS_2 nanosheets were created on the basis of MoS_2 supercells with various layer thicknesses. The interlayer van der Waals interactions (vdWs) in pristine and lithiated MoS_2 nanosheets were correlated using PBE functional with the vdWs dispersion correction (DFT-D2) for accuracy. Brillouin Zone (BZ) integrations were performed on a grid of (5 × 5 × 1) Monkhorst–Pack k-point sets. Ultrasoft pseudopotentials were

utilized along with a plane-wave cut-off energy of 400 eV. For geometry optimization, the convergence criteria of electronic and ionic interactions were set as 10^{-3} and 10^{-2} eV·Å^{-1}, respectively. More details are presented in the supporting information.

The thermodynamic phase diagrams were calculated following a previous report with some modifications. For the formation of Li-Mo-S ternary compounds, the chemical potential of Li, Mo, and S should satisfy the following equation:

$$\Delta\mu_{Li} + \Delta\mu_{Mo} + \Delta\mu_{S} = \Delta E_f\,(Li_xMo_yS_{2y})$$

where $\Delta\mu_{Li}$, $\Delta\mu_{Mo}$ and $\Delta\mu_{S}$ are the chemical potentials of Li, Mo, and S referring to their bulks, respectively. $\Delta E_f\,(Li_xMo_yS_{2y})$ is the formation energy of Li-Mo-S ternary compounds. (See details in Table S1) In order to avoid the formation of elementary substances of Li, Mo, or S, the chemical potential of elements should satisfy the following condition:

$$\Delta\mu_{Li} \leq 0;\ \Delta\mu_{Mo} \leq 0;\ \Delta\mu_{S} \leq 0$$

Furthermore, the chemical potential of Li, Mo, and S should obey the following equation to avoid the formation of secondary Li_2S and MoS_2:

$$2\Delta\mu_{Li} + \Delta\mu_{S} \leq \Delta E_f\,(Li_2S);\ \Delta\mu_{Mo} + 2\Delta\mu_{S} \leq \Delta E_f\,(MoS_2)$$

where $\Delta E_f\ (Li_2S)$ and $\Delta E_f\ (MoS_2)$ are the formation energy of Li_2S and MoS_2, respectively.

The adsorption energy (E_a) between 1T-MoS_2 and polysulfide species (L_2S_4 or L_2S_6) was calculated according to the following equation:

$$E_a = E_s - \Delta E_f\,(MoS_2) - \Delta E_f\,(Li_2S_4 \text{ or } Li_2S_6)$$

where E_s is the total energy of system, while $\Delta E_f\,(MoS_2)$ and $\Delta E_f\,(Li_2S_4$ or $Li_2S_6)$ are

the formation energies of 1T-MoS_2 and polysulfide species (L_2S_4 or L_2S_6), respectively. The formation energies of 1T-MoS_2, 2H-MoS_2 and lithiated 1T-MoS_2 and 2H-MoS_2 with various layer numbers are listed in Table S1.

Supplementary Figures and Tables

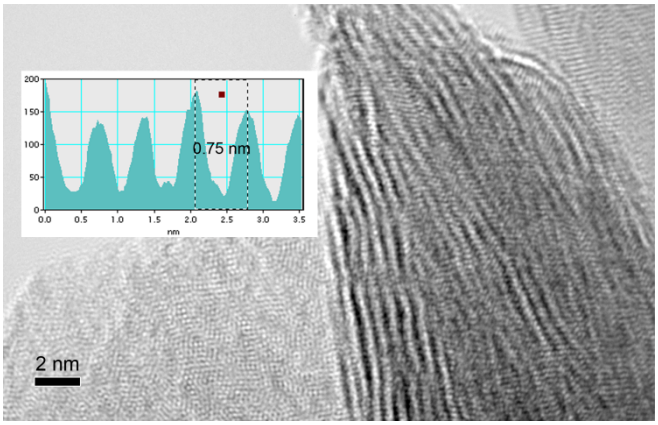

Fig. S1 HRTEM image of the lateral view of 1T-MoS_2.

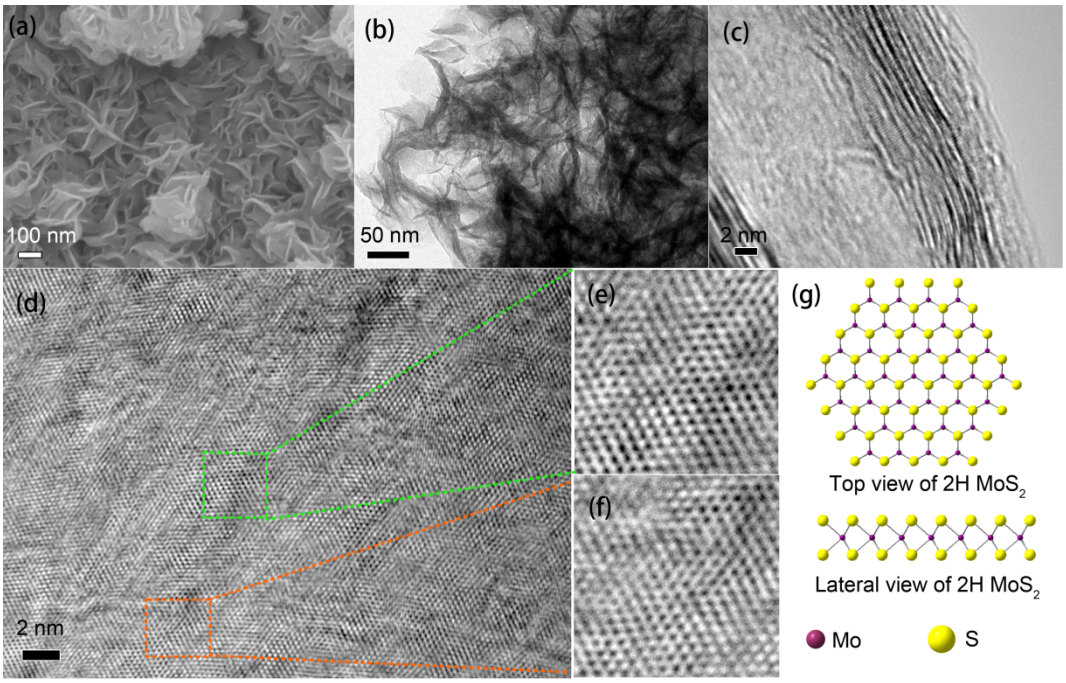

Fig. S2 Morphological characterization of 2H-MoS_2/Ti. (a) SEM and (b-d) (HR)TEM images. (e, f) zoom-in view of the selected region in the HRTEM image of (d); (g) crystal structure of 2H-MoS_2.

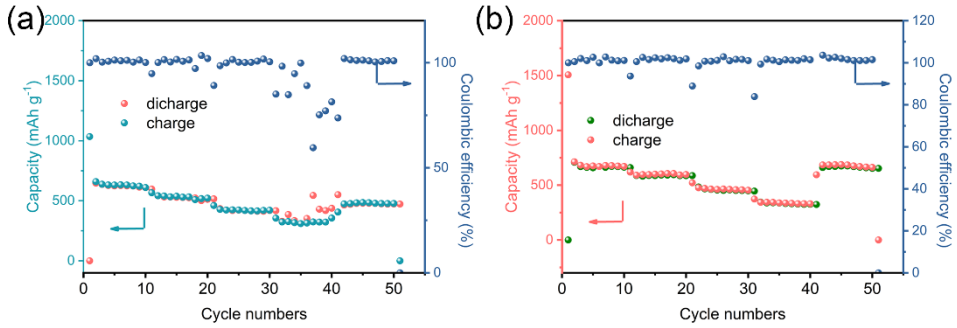

Fig. S3 Rate performance of (a) 2H-MoS_2/Ti and (b) 1T-MoS_2/Ti under current densities of 100, 200, 300 and 500 mA·mg^{-1} and then recovered to 100 mA·mg^{-1}.

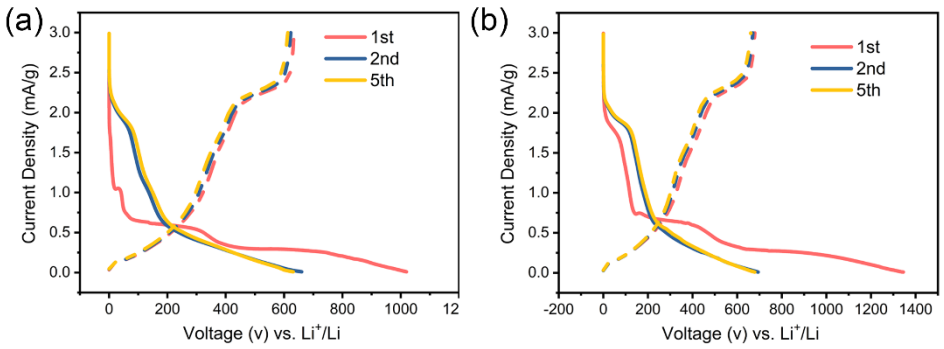

Fig. S4 Charge-discharge curves of 2H-MoS_2/Ti and 1T-MoS_2/Ti under a current density of 100 $mA \cdot mg^{-1}$.

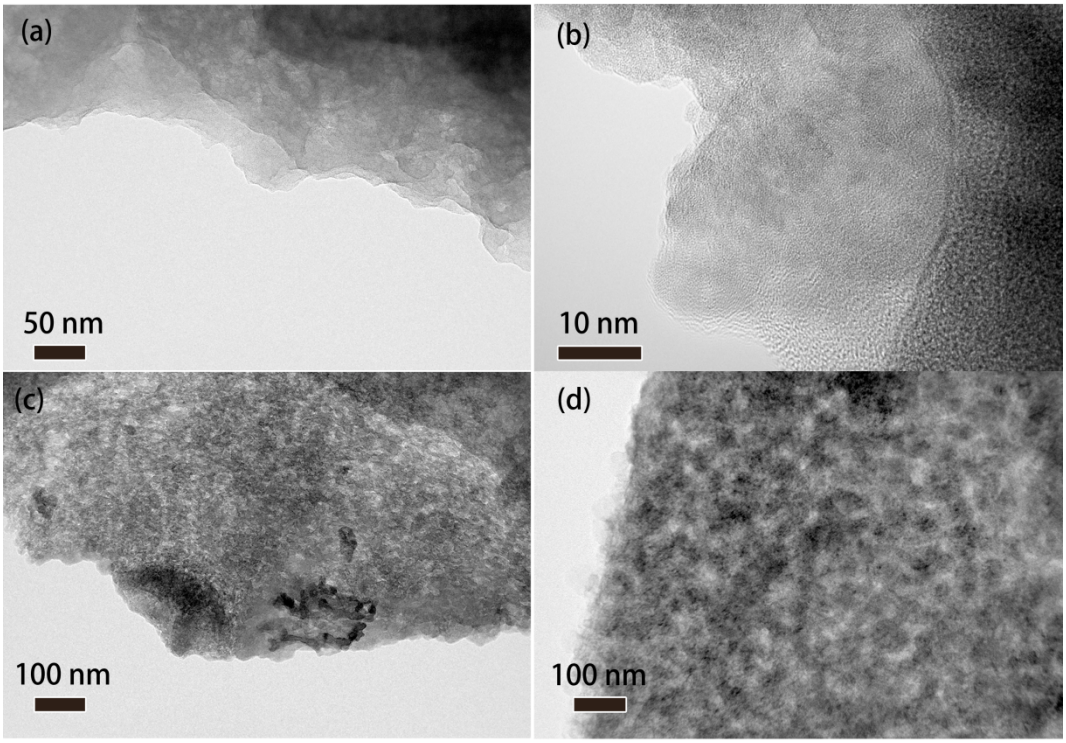

Fig. S5 Morphological characterization of the exfoliation from the electrodes cycled for various times. TEM images of the exfoliation from (a) 2H-MoS_2/Ti after the initial discharge process and (b) the recharged process. (c) 1T-MoS_2/Ti after the initial discharge and (d) the recharged process.

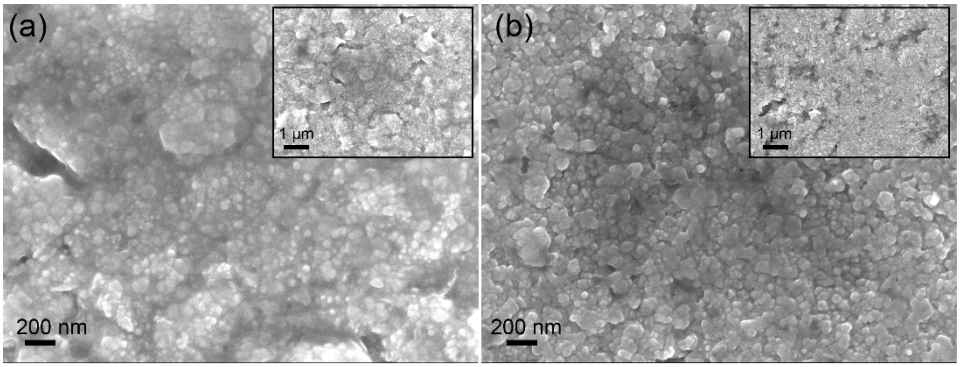

Fig. S6 Morphological characterization (a) 2H-MoS_2/Ti and (b) 1T-MoS_2/Ti after initial 5 charge-discharge cycles.

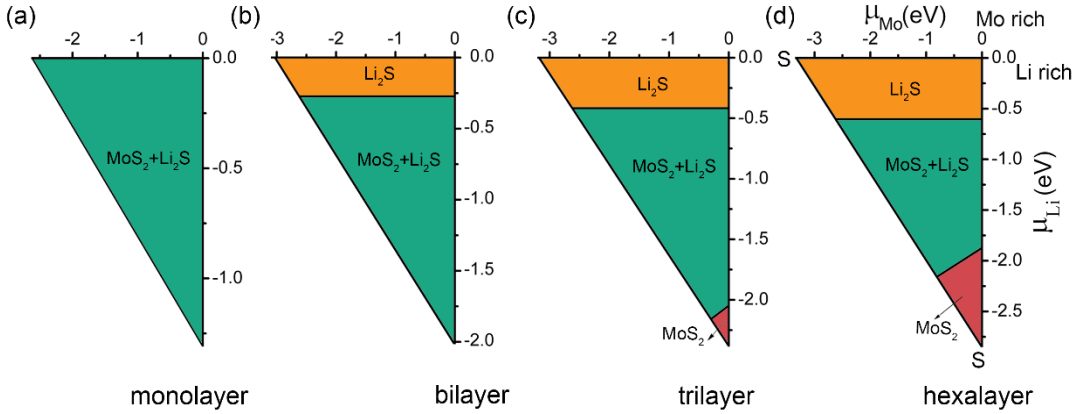

Fig. S7 Thermodynamic phase diagram of lithiated 2H MoS_2 with various layer numbers.

Table S1. The formation energies of 1T-MoS_2, 2H-MoS_2 and lithiated 1T-MoS_2 and 2H-MoS_2 with various layer numbers.

Species	Formation Energy (eV)
Li(1)	0
Mo(1)	0
S(32)	0
Li_2S(1)	-4.317
2H-MoS_2(1)	-2.620
1T-MoS_2(1)	-1.811
1Layer-2H-MoS_2(Li_2MoS_2)	-2.619
2Layer-2H-MoS_2($Li_3Mo_2S_4$)	-6.059
3Layer-2H-MoS_2($Li_4Mo_3S_6$)	-9.529
6Layer-2H-MoS_2($Li_7Mo_6S_{12}$)	-19.949
1Layer-1T-MoS_2(Li_2MoS_2)	-2.963
2Layer-1T-MoS_2($Li_3Mo_2S_4$)	-6.781
3Layer-1T-MoS_2($Li_4Mo_3S_6$)	-14.262
6Layer-1T-MoS_2($Li_7Mo_6S_{12}$)	-29.213